TECHNICAL ARTICLE

Host–guest adsorption behavior of deuterated methane and molecular oxygen in a porous rare-earth metal–organic framework

Stephen H. Ogilvie,[1] Samuel G. Duyker,[2] Peter D. Southon,[1] Vanessa K. Peterson,[2] and Cameron J. Kepert[1,a)]
[1]*School of Chemistry, The University of Sydney, NSW 2006, Australia*
[2]*Australian Nuclear Science and Technology Organisation, NSW, Australia*

(Received 5 September 2014; accepted 19 September 2014)

The yttrium-based metal–organic framework, Y(btc) (btc = 1,3,5-benzenetricarboxylate), shows moderate uptake of methane (0.623 mmol g^{-1}) and molecular oxygen (0.183 mmol g^{-1}) at 1 bar and 308 K. Neutron powder-diffraction data for the guest-free, CD_4-, and O_2-loaded framework reveal multiple adsorption sites for each gas. Both molecular guests exhibit interactions with the host framework characterised by distances between the framework and guest atoms that range from 2.83 to 4.81 Å, with these distances identifying interaction most commonly between the guest molecule and the carboxylate functional groups of the benzenetricarboxylate bridging ligand of the host. © *2014 International Centre for Diffraction Data.* [doi:10.1017/S0885715614001158]

Key words: adsorption, metal–organic frameworks, neutron powder diffraction, adsorption behaviour

I. INTRODUCTION

Metal–organic frameworks (MOFs) are a class of porous, crystalline coordination networks that have generated a great deal of interest as a result of their range of interesting properties. The relative ease of chemical and structural modification enables tuning of these properties, which include anomalous thermal expansion as a result of structural flexibility (Goodwin *et al.*, 2008), guest-dependent spin crossover behaviour (Halder *et al.*, 2002), and effects of pore environment on gas adsorption (McDonald *et al.*, 2011). The latter, in combination with the high surface area of MOFs – as much as 5000 m^2 g^{-1} (D'Alessandro *et al.*, 2010) – has motivated substantial research in recent years to investigate the suitability of these materials for use as adsorbents in the separation and storage of gases, including energy-carriers such as hydrogen and methane. The separation and storage of methane using MOFs are of particular relevance for natural-gas energy systems when implemented as replacements for costly cryogenic or dangerous high-pressure containment vessels (Tagliabue *et al.*, 2011). Oxygen separation using MOFs may find applications in oxyfuel combustion processes, which involve combustion in the presence of pure O_2, generating an exhaust stream with a much higher CO_2 content (80–98%) compared with that produced from combustion in air, thus simplifying the sequestration of the resultant CO_2 (Metz *et al.*, 2005). In this regard, MOFs have been presented as a means with which to perform the O_2/N_2 separation required for oxyfuel combustion systems (Bloch *et al.*, 2011), where the energy penalty for oxyfuel processes is reduced alongside the generation of the required concentrated O_2 source.

In this work, we report the structural mechanism for methane and oxygen sorption by the desolvated yttrium-based MOF, Y(btc) (btc = 1, 3, 5 benzenetricarboxylate). Y(btc), see Figure 1, is a three-dimensional framework with the MOF-76 structure (Rosi *et al.*, 2005), containing porous channels of approximately 5.8 × 5.8 $Å^2$ that run parallel to the *c*-axis (Luo *et al.*, 2008). These channels provide an attractive environment for guest molecules as they are lined with both bridging-ligand features and coordinatively-unsaturated metal sites. Previous studies have shown that MOFs containing accessible functional groups (Das *et al.*, 2012) and bare-metal sites (Ogilvie *et al.*, 2013) demonstrate enhanced uptake of guest molecules, obtained through both strengthened host–guest interactions and increased adsorption selectivity.

For this research, neutron powder diffraction (NPD) was employed to elucidate the sorption mechanism of deuterated methane and molecular oxygen within Y(btc). The detailed structural analysis of the binding of these guests in Y(btc) has helped develop current understandings of the host–guest interactions that underpin and influence both the ability and capacity of MOFs to absorb and release these molecules.

II. EXPERIMENTAL

A. Preparation of Y(btc)

$Y(NO_3)_3{\cdot}6H_2O$ (5.22 g, 13.63 mmol) and 1,3,5 benzenetricarboxylic acid (1.06 g, 5.04 mmol) were dissolved in a mixture of dimethylformamide (80 ml), ethanol (80 ml), and H_2O (80 ml) at room temperature. The mixture was divided into four 100 ml Parr Teflon-lined vessels and heated at a rate of 1.1 K min^{-1} before holding at 363 K for 18 h to yield colourless needle-shaped crystals (2.3119 g). The sample was then allowed to cool naturally before being vacuum filtered, washed with ethanol (100 ml), and ground to a fine white powder. Desolvation (activation) of the sample was achieved by heating in a glass sample tube at 573 K under high vacuum (~10^{-5} mbar).

a)Author to whom correspondence should be addressed. Electronic mail: cameron.kepert@sydney.edu.au

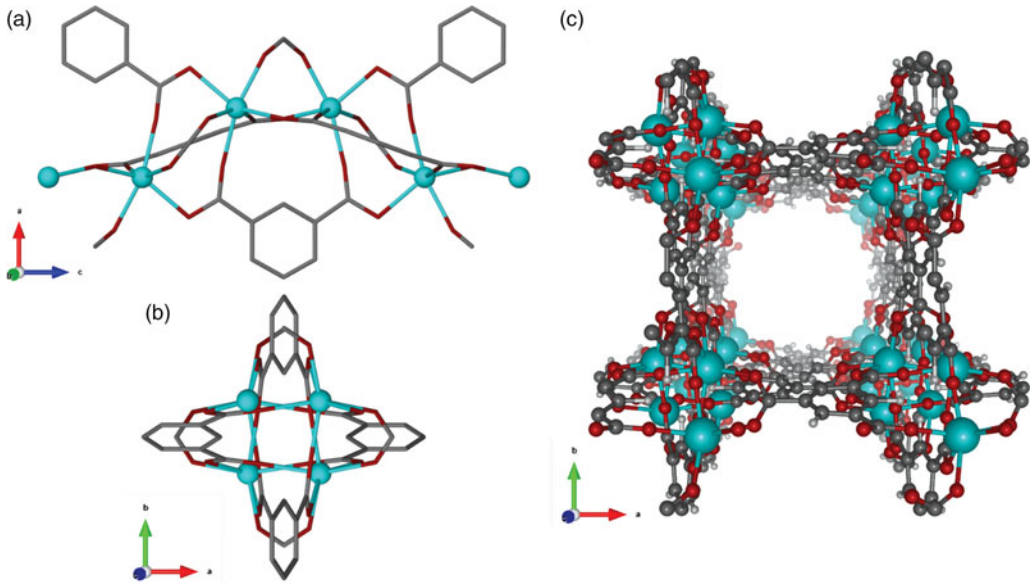

Figure 1. (Color online) Tetragonal network of the desolvated Y(btc) metal–organic framework. (a) Unit cell as viewed along the *b*-axis, (b) unit cell as viewed along the *c*-axis, and (c) extended network demonstrating accessible pore space. Shown are Y (blue), C (dark grey), and O (red). H (light grey) are omitted for clarity from (a) and (b) and shown in (c).

B. Gas adsorption measurement

CH_4 and O_2 adsorption isotherms were measured using a Hiden-Isochema IGA-002 gravimetric system. Freshly desolvated material was loaded into a stainless steel basket and heated to 368 K under high vacuum ($<10^{-6}$ mbar) for 10 h, at which point the mass was stable (approx. 48 mg). Isotherms were measured at 308 K, with the temperature maintained within 0.1 K.

C. Neutron powder diffraction

Prior to NPD measurements and gas dosing, the activated sample was transferred to a cylindrical vanadium can (internal diameter 6 mm) inside a helium-filled glovebox equipped with water and oxygen monitors. The sample cell was then connected to a custom-designed gas-delivery centrestick and inserted into a top-loading cryofurnace with the sample and thermally isolated capillary line under vacuum. NPD data were collected on the high-resolution neutron diffractometer ECHIDNA (Liss *et al.*, 2006) at the Australian Nuclear Science and Technology Organisation (ANSTO) using a wavelength of 2.4425 Å. An initial diffraction pattern (7.5 h) was collected for the empty sample (1.376 g) at 10 K to be used as a structural reference from which subsequent structures of the sample dosed with methane and oxygen may be refined. The sample was then dosed with a known amount of gaseous guest, using a manual gas-dosing device comprising a calibrated dosing volume and high-accuracy pressure transducer, at 240 K and slowly cooled to 200 K at which point the pressure in the system had decreased to zero. The sample was then cooled over 1 h to the measurement temperature of 10 K. The relatively fast adsorption kinetics for these guests meant that adsorption occurred relatively early during the cooling process, ensuring that each guest diffused through the sample and reached their thermodynamic equilibrium position prior to being "locked in" at lower temperatures as a result of significantly reduced thermal motion. No evidence was found in the diffraction patterns that suggested any guest had solidified and when coupled with the zero pressure reading, it was inferred that all the guests had been adsorbed by the sample. Diffraction data were collected over 5 h for guest doses of 1.00 CD_4:Y and 1.00 O_2:Y in Y(btc), with a re-activation performed by evacuation at 350 K for 1 h between guests.

D. Structural analysis

Rietveld refinements were performed using GSAS (Larson and Von Dreele, 1994) as implemented in EXPGUI (Toby, 2001). For each refinement, a 12-term shifted Chebyshev background function and pseudo-Voigt peak profile with asymmetry (CW neutron Type III in GSAS) was used. Prior to each refinement, a Le Bail extraction was performed to refine unit-cell parameters, which were then kept constant during the subsequent Rietveld refinement. For all data for gas-loaded samples, all reflections were indexed by the original $P4_322$ space group and the refined structure of the empty framework was used as the starting model for the guest-loaded structures. For the guest-loaded structure, atom parameters for the empty framework were refined and guest molecule locations determined from Fourier-difference maps that were visualised using the program VESTA (Momma and Izumi, 2011). All guests were modelled as complete molecules in the Rietveld refinements. Guest-loaded Y(btc) structures could not be adequately described without including guests in the structural model, with the weighted profile factor (R_{wp}) improving by 20–25% upon their inclusion. All host–guest and guest–guest distances were considered in conjunction with site occupancy factors (SOFs) to ensure that physically realistic results were obtained.

III. RESULTS AND DISCUSSION

A. Y(btc) gas-adsorption isotherms

Prior to gas-adsorption measurements, the sample was heated under vacuum to ensure the sample was thoroughly desolvated, including the removal of coordinated water

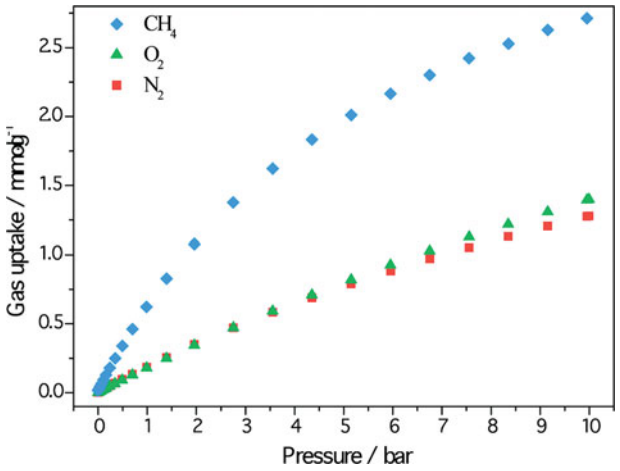

Figure 2. (Color online) Adsorption isotherms for CH_4 (blue diamonds), O_2 (green triangles), and N_2 (red squares) at 308 K.

molecules that occupy the bare-metal sites upon synthesis. The complete removal of water from the framework ensures access to both pore space and bare-metal sites for guest molecules during gas adsorption. Adsorption isotherms for methane, oxygen, and nitrogen gas at 308 K are shown in Figure 2. The CH_4 uptake at 1 and 10 bar was found to be 0.623 and 2.714 mmol g^{-1}, respectively, with O_2 uptake at 1 and 10 bar found to be 0.183 and 1.399 mmol g^{-1}, respectively.

B. Binding of deuterated methane in Y(btc)

Analysis of NPD data (Tables I and II) for the CD_4-loaded material at 10 K reveals two adsorption sites, labelled A_{CD4} and B_{CD4}, as shown in Figure 3. In the first of these, site A_{CD4}, the CD_4 is found to most strongly interact with the carboxylate functional groups of the btc bridging ligand of the host framework. These interactions occur at distances from the C of the CD_4 in the range of 3.079–3.595 Å from the O atoms and 3.457 Å from the C atoms of the carboxylate functional group. Site B_{CD4} is seen to occupy a similar site to that of site A_{CD4}, whereby the nearest carboxylate–CD_4 distances range from 3.454 to 3.474 Å. This site also demonstrates an interaction with the benzene ring of the btc bridging ligand, most likely as a result of the good match between the pore shape and the methane guest, with the acute angle between adjacent btc ligands providing a significant surface area with which methane can interact.

We note that neither of these adsorption sites display interaction with the available bare-metal sites of the host framework. Instead, each site is seen to have nearest host–guest distances with the bridging btc ligand, particularly with the carboxylate functional groups. Based on these observations, it likely that the density, partial charge, and availability of adjacent carboxylate groups provide a location for guest methane molecules to adsorb that is more favourable than the bare-metal sites. Refined SOFs for the methane atoms yield a total of 0.668(48) CD_4 molecules per Y atom (see Table I), falling short of the 1 CD_4:Y dose, likely as a result of positional disorder of the remaining CD_4 molecules.

When considering the occupancies of each site, it is important to note the proximity of neighbouring sites to one another. Since each site generates a symmetrically equivalent nearest neighbour that is either 1.784 Å (site A_{CD4}) or 1.902 Å (site B_{CD4}) away, eight pairs of symmetrically equivalent molecules are generated per unit cell between the two sites. Therefore, to maintain physically reasonable intermolecular distances, a maximum of one CD_4 molecule is allowed per pair, resulting in a maximum of eight CD_4 molecules per unit cell and equivalent to two CD_4:Y, if only the observed sites are considered. The refined SOFs are in agreement with this, and the similar refined occupancies of site A_{CD4} [0.394 (40) CD_4:Y] and site B_{CD4} [0.274(8) CD_4:Y] suggest little difference in the favourability of each site for methane, which is consistent with the similar nature of the host–guest interactions at each site.

C. Binding of molecular oxygen in Y(btc)

Analysis of NPD data collected for the O_2-loaded sample reveals three distinct O_2 adsorption sites in Y(btc), labelled A_{O2}, B_{O2}, and C_{O2}, as shown in Figure 4. Site A_{O2} is observed to have the highest refined occupancy [0.722(16) O_2:Y], more than triple that of site B_{O2} [0.220(14) O_2:Y] and C_{O2} [0.198 (10) O_2:Y]. The total observed O_2:Y = 1.14(40) is in good agreement with the delivered dose of 1.00 O_2:Y. The larger value and better agreement relative to the CD_4-loaded structure suggests that the O_2 guest may be more localised. When distances between neighbouring O_2 molecules are considered, the maximum number of molecules allowed per unit cell corresponds to the total number of symmetry-generated locations for each observed site, yielding 16 O_2 molecules per unit cell and equivalent to four O_2 molecules per Y. The higher occupation of site A_{O_2} therefore suggests that this site is the preferred binding site for O_2 in Y(btc), with this and the next most occupied site, B_{O_2}, broadly consistent with the type of interaction that was seen in the CD_4-loaded samples, where the closest CD_4–carboxylate distances are between 3.190 and 3.473 Å. However, molecular oxygen appears to have stronger interactions with the aromatic ring of the bridging ligand, as evidenced by shorter host–guest distances of 2.831 to 3.111 Å.

Site C_{O_2} is the only site for either guest that exhibits significant interaction with the bare-metal site available in this framework. At this site, the oxygen molecule interacts with the bare-metal site in a side-on fashion, with both O atoms being an equivalent distance (3.77 Å) from the Y centre.

TABLE I. Unit-cell parameters and site occupancy factors determined using Rietveld analysis of NPD data for guest-free Y(btc), as well as CD_4- and O_2-loaded Y(btc).

Guest	Unit-cell parameter $a = b$	Unit-cell parameter c	Observed site A	Observed site B	Observed site C	Observed A + B + C	R_{wp} (%)
None	10.2998(1)	13.8635(2)	–	–	–	0	3.46
CD_4	10.2970(2)	13.8581(3)	0.394(40)	0.274(8)	–	0.668(48)	4.85
O_2	10.2974(3)	13.8600(5)	0.722(16)	0.220(14)	0.198(10)	1.140(40)	5.58

TABLE II. Structural details determined by the Rietveld analysis of NPD data for Y(btc), as well as CD_4 and O_2 sites within Y(btc).

	Atom	Site	Fractional coordinates			Atomic displacement parameter (U_{iso})/10^{-2} A^2
			x	*y*	*z*	
	Y1	4*c*	0.3763(4)	0.3763(4)	0.125	1.15(18)
	O1	8*d*	0.2340(6)	0.4153(7)	1.0013(5)	4.16(23)
	O2	8*d*	0.4160(5)	0.4091(6)	0.9118(4)	1.93(18)
	O3	8*d*	0.8131(4)	0.5859(5)	0.6995(4)	1.18(17)
	C1	4*b*	0.2806(3)	0.5	0.75	1.15(16)
Y(btc) structure	H1A	4*b*	0.387(1)	0.5	0.75	4.74(47)
	C2	8*d*	0.2158(2)	0.4584(5)	0.8332(1)	1.75(15)
	C3	8*d*	0.0832(3)	0.4590(4)	0.8332(1)	1.55(14)
	H3A	8*d*	0.0362(8)	0.4293(8)	0.8996(5)	1.01(23)
	C4	4*b*	0.0202(3)	0.5	0.75	0.64(19)
	C5	8*d*	0.2982(4)	0.4232(5)	0.9216(3)	1.82(16)
	C6	4*b*	0.8700(6)	0.5	0.75	0.58(2)
	C7	8*d*	0.168(1)	0.917(2)	0.218(1)	11.7(13)
	D1	8*d*	0.254(3)	0.895(5)	0.247(3)	11.7(13)
	D2	8*d*	0.183(3)	0.958(3)	0.159(2)	11.7(13)
	D3	8*d*	0.126(4)	0.837(3)	0.194(3)	11.7(13)
	D4	8*d*	0.113(3)	0.967(4)	0.258(1)	11.7(13)
CD_4 sites	C8	8*d*	0.824(4)	0.736(5)	0.067(5)	37.1(24)
	D5	8*d*	0.877(13)	0.668(13)	0.030(14)	37.1(24)
	D6	8*d*	0.849(8)	0.826(15)	0.037(14)	37.1(24)
	D7	8*d*	0.857(10)	0.736(20)	0.133(5)	37.1(24)
	D8	8*d*	0.728(4)	0.721(6)	0.067(14)	37.1(24)
O_2 sites	O4	8*d*	0.116(2)	0.740(2)	0.075(2)	9.2(8)
	O5	8*d*	0.161(2)	0.843(2)	0.106(2)	9.2(8)
	O6	8*d*	0.801(6)	0.719(7)	0.103(8)	19.9(44)
	O7	8*d*	0.891(5)	0.876(5)	0.585(3)	12.2(26)

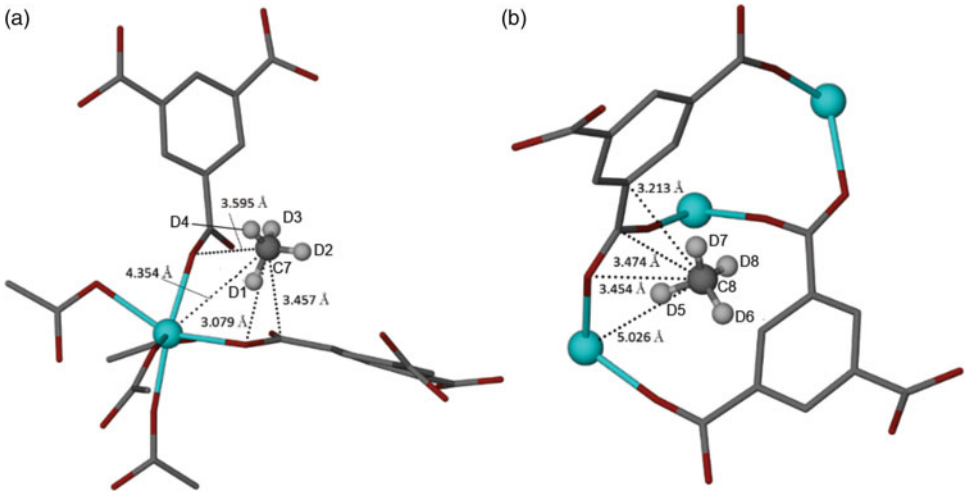

Figure 3. (Color online) Deuterated methane adsorption sites (a) A_{CD4} and (b) B_{CD4}, demonstrating nearest framework–guest interactions. Shown are Y (blue), C (dark grey), O (red), and D (light grey). Framework H atoms are omitted for clarity.

This motif effectively maximises the simultaneous interaction of each O atom with the charged surface of the bare-metal site. Despite site C_{O_2} having the only observable interaction with this bare-metal site, there is no notable lengthening of the O = O bond, as one might expect. A similar symmetric side-on interaction has previously been reported in Fe_2(dobdc) (Bloch *et al.*, 2011). However, there are a few notable differences between these two examples. Firstly, in the Fe_2(dobdc) system, this side-on interaction is observed to have the highest occupancy of three distinct O_2-adsorption sites within the framework, as opposed to having the lowest occupancy in this Y(btc) framework. Secondly, the Fe_2(dobdc) system displays a much shorter *M*–O_2 interaction distance of *ca.* 2.10 Å, compared with 3.77 Å in Y(btc). The differences in O_2 binding for these two frameworks are attributed partly to the differences in chemistry of Fe^{II} and Y^{III}, but also to the different coordination geometries of the metal cations, which affect their accessibility. The coordination spheres of the Y cation in both solvated and desolvated Y(btc) are shown in Figure 5. Upon removal of the coordinated water molecule, a reduction in the angles between opposing carboxylate O atoms effectively limits the ability for guest species to approach and

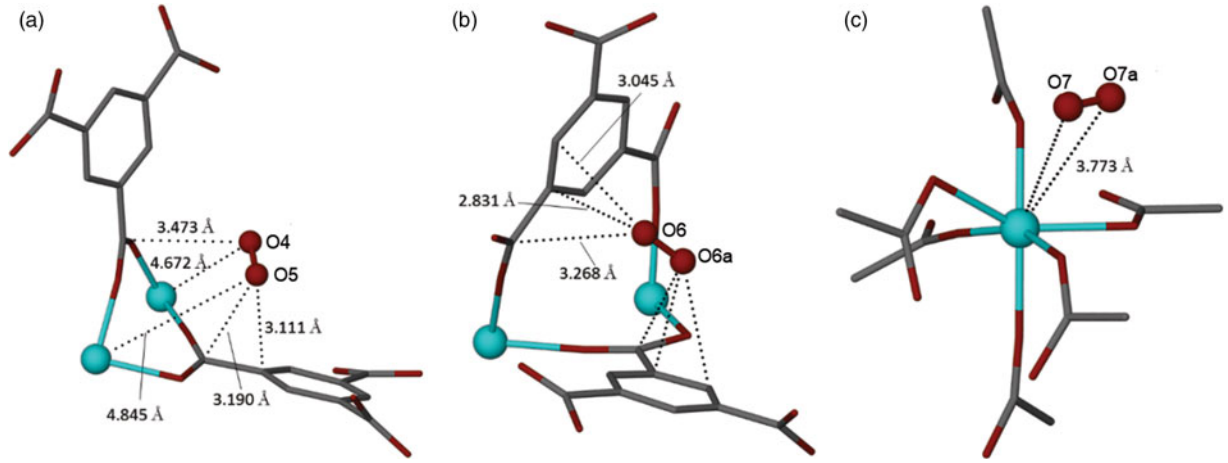

Figure 4. (Color online) O_2 adsorption sites (a) A_{O2}, (b) B_{O2}, and (c) C_{O2}, demonstrating nearest framework–guest distances. Shown are Y (blue), C (dark grey), and O (red). Framework H atoms are omitted for clarity. A lower-case letter following the atom label has been used to demonstrate symmetrically equivalent atoms.

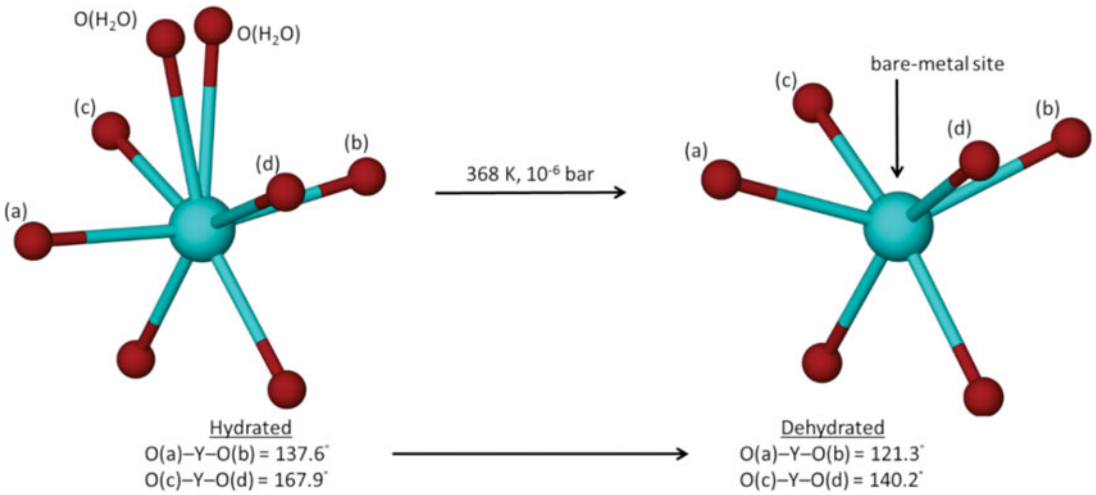

Figure 5. (Color online) Geometric changes in the coordination sphere of the Y centre upon desolvation, yielding a bare-metal site. In the hydrated phase, the H_2O molecule is disordered over two positions. Shown are Y (blue) and O (red).

interact with the metal site. These O–Y–O angles are as small as 121° in Y(btc), contrasting with the square pyramidal Fe coordination in Fe_2(dobdc) with O–Fe–O angles of approximately 180°. These steric effects may be responsible for precluding interaction with the CD_4 molecules while allowing some interaction with the smaller O_2 molecules. It is the limited accessibility of the Y cation in the desolvated framework that likely results in the btc ligand interactions being the main driver of both CD_4 and O_2 binding.

IV. CONCLUSIONS

In conclusion, we have characterised the adsorption of both CH_4 and O_2 within the MOF Y(btc), which displays uptakes of 0.623 and 0.183 mmol g^{-1}, respectively, at 1 bar. Analysis of NPD data from the guest-loaded framework has revealed two adsorption sites for deuterated methane and three sites for molecular oxygen. The majority of guest interactions with the framework structure appear to involve the carboxylate functional groups of the bridging ligand with guest–framework distances in the range 3.2–3.5 Å. Interestingly, interactions with available bare-metal metal sites within the framework are either weak (for molecular oxygen) or non-existent (for methane). This is attributed to the contraction in O–Y–O coordination angles upon desolvation of the Y (btc) and removal of the coordinated water molecule, limiting the accessibility of the Y cation to guest molecules. This work reveals the importance of considering the accessibility of bare-metal sites in porous framework materials, in conjunction with their known attractiveness for guests, when assessing their effectiveness as sorbents.

ACKNOWLEDGEMENTS

This research was supported by the Science and Industry Endowment Fund, the Australian Research Council, and an Australian Institute of Nuclear Science and Engineering Postgraduate Research Award. Research is supported by the Australian Nuclear Science and Technology Organisation's Energy Materials project. We thank the sample environment team at the Australian Nuclear Science and Technology Organisation for help with preparing the gas-delivery equipment used in the experiment.

Bloch, E. D., Murray, L. J., Queen, W. L., Chavan, S., Maximoff, S. N., Bigi, J. P., Krishna, R., Peterson, V. K., Grandjean, F., Long, G. J., Smit, B., Bordiga, S., Brown, C. M., and Long, J. R. (**2011**). "Selective binding of O_2 over N_2 in a redox-active metal-organic framework with open iron(II) coordination sites," J. Am. Chem. Soc. **133**, 14814–14822.

D'Alessandro, D. M., Smit, B., and Long, J. R. (**2010**). "Carbon dioxide capture: prospects for new materials," Angew. Chem., Int. Ed. **49**, 6058–6082.

Das, A., Southon, P. D., Zhao, M., Kepert, C. J., Harris, A. T., and D'Alessandro, D. M. (**2012**). "Carbon dioxide adsorption by physisorption and chemisorption interactions in piperazine-grafted Ni_2(dobdc) (dobdc = 1,4-dioxido-2,5-benzenedicarboxylate),"Dalton Trans. **41**, 11739–11744.

Goodwin, A. L., Calleja, M., Conterio, M. J., Dove, M. T., Evans, J. S. O., Keen, D. A., Peters, L., and Tucker, M. G. (**2008**). "Colossal positive and negative thermal expansion in the framework material $Ag_3[Co(CN)_6]$," Science **319**, 794–797.

Halder, G. J., Kepert, C. J., Moubaraki, B., Murray, K. S., and Cashion, J. D. (**2002**). "Guest-Dependent spin crossover in a nanoporous molecular framework material," Science **298**, 1762–1765.

Larson, A. C. and Von Dreele, R. B. (**1994**). General Structure Analysis System (GSAS), Los Alamos National Laboratory Report LAUR 86–748.

Liss, K.-D., Hunter, B., Hagen, M., Noakes, T., and Kennedy, S. (**2006**). "Echidna-the new high-resolution powder diffractometer being built at OPAL," Physica B **385–386**, 1010–1012.

Luo, J., Xu, H., Liu, Y., Zhao, Y., Daemen, L. L., Brown, C., Timofeeva, T. V., Ma, S., and Zhou, H.-C. (**2008**). "Hydrogen adsorption in a highly stable porous rare-earth metal-organic framework: sorption properties and neutron diffraction studies," J. Am. Chem. Soc. **130**, 9626–9627.

Mcdonald, T. M., D'Alessandro, D. M., Krishan, R., and Long, J. R. (**2011**). "Enhanced carbon dioxide capture upon incorporation of N, N'-dimethylethylenediamine in the metal-organic framework CuBTTri," Chem. Sci. **2**, 2022–2028.

Metz, B., Davidson, O., Coninck, H. D., and Loos, L. M. (**2005**). "IPCC, 2005: IPCC Special Report on Carbon Dioxide Capture and Storage. Prepared by Working Group III of the Intergovernmental Panel on Climate Change" [Metz, B., O. Davidson, H. C. de Coninck, M. Loos, and L. A. Meyer (eds.)]. Cambridge University Press, Cambridge, United Kingdom and New York, NY, USA, 442 pp.

Momma, K. and Izumi, F. (**2011**). "VESTA 3 for three-dimensional visualization of crystal, volumetric and morphology data," J. Appl. Crystallogr. **44**, 1272–1276.

Ogilvie, S. H., Duyker, S. G., Southon, P. D., Peterson, V. K., and Kepert, C. J. (**2013**). "Identification of bridged CO2 binding in a Prussian blue analogue using neutron powder diffraction," Chem. Commun. **49**, 9404–9406.

Rosi, N. L., Kim, J., Eddaoudi, M., Chen, B., O'Keefe, M., and Yaghi, O. M. (**2005**). "Rod packings and metal-organic frameworks constructed from rod-shaped secondary building units," J. Am. Chem. Soc. **127**, 1504–1518.

Tagliabue, M., Rizzo, C., Millini, R., Dietzel, P. D. C., Blom, R., and Zanardi, S. (**2011**). "Methane storage on CPO-27-Ni pellets," J. Porous Mater. **18**, 289–296.

Toby, B. H. (**2001**). "EXPGUI, a graphical user interface for GSAS," J. Appl. Crystallogr. **34**, 210–213.